Ore Geology Reviews 158 (2023) 105530

Contents lists available at ScienceDirect

Ore Geology Reviews

journal homepage: www.elsevier.com/locate/oregeorev

The Zunyi manganese deposit, South China: A consequence of climatic-oceanic changes triggered by the eruption of Emeishan large Igneous Province?

Chuang Yang [a,b], Hai Xu [c,d], Runsheng Yin [a,*], Li Wang [a,e], Chengquan Wu [a], Stephen E. Grasby [f], Junbo Gao [c,d,*]

[a] State Key Laboratory of Ore Deposit Geochemistry, Institute of Geochemistry, Chinese Academy of Sciences, Guiyang 550081, China
[b] University of Chinese Academy of Sciences, Beijing 100049, China
[c] College of Resources and Environmental Engineering, Guizhou University, Guiyang 550025, China
[d] Key Laboratory of Karst Georesources and Environment, Ministry of Education, Guizhou University, Guiyang 500025, China
[e] Institute of Sedimentary Geology, Chengdu University of Technology, Chengdu 610059, China
[f] Geological Survey of Canada, Natural Resources Canada, 3303 33rd St NW, Calgary, AB, Canada

ARTICLE INFO

Keywords:
The Zunyi manganese deposit
Middle Permian
Climatic-oceanic changes
Emeishan Large Igneous Province

ABSTRACT

South China hosts a large number of Middle Permian marine sedimentary Mn deposits (MSMDs) coeval to the eruption of the Emeishan Large Igneous Province (ELIP). The linkage between these MSMDs and ELIP eruption remains unclear. Here, we observed anomalously high Hg concentrations and Hg/TOC ratios, and a shift of Δ^{199}Hg to near-zero at the base of the Middle Permian Zunyi MSMD. These results suggest ELIP eruption as a possible driving force for the deposition of the Zunyi MSMD. Principal component analysis (PCA) of trace element concentrations of the Zunyi MSMD samples revealed three clusters of trace elements. Cluster A elements (Cr, Zn, Mo, Sb, and Tl) are anomalously high at the basal of the Zunyi MSMD, confirming ELIP as a driver for the formation of this deposit. Cluster B elements (Ba, Rb, and Cu) are high in the entire deposit, supporting elevated oceanic productivity. A stepwise increase in Cluster C elements (Li, Ga, Sn, Zr, Nb, Hf, Ta, and W) concentrations in the Zunyi MSMD suggests enhanced terrestrial weathering. We infer that the ELIP eruption triggered an increased input of terrestrial nutrients to the ocean, causing increased oceanic productivity and rising dissolved O_2 levels in the surface water of the middle Permian ocean in South China, favoring Mn deposition and MSMDs formation.

1. Introduction

Manganese (Mn), an essential metal widely used in industry, is denoted as a critical metal in China, the United States, European Union, Australia, along with many other countries (Entr, 2014; Tang et al., 2014). In nature, Mn occurs with three oxidation states (+2, +3, +4) (Thamdrup et al., 2000). Dissolved Mn^{2+} species exist mainly in oxygen-poor waters, whereas insoluble Mn^{3+} and Mn^{4+} species are dominant in oxidized waters (Hem, 1972). The mobilization and transportation of Mn favor the presence of oxygen-poor waters, whereas the deposition of Mn occurs in oxygen-rich waters (Murray et al., 1985). Marine sedimentary Mn deposits (MSMDs) host the world's largest Mn mineral resources, and their formation was governed by changes in seawater redox conditions throughout geological history (Post,1999; Armstrong, 2008).

Large numbers of MSMDs were formed in South China during the Middle Permian, however, their origin remains controversial. Amongst these deposits, the Zunyi MSMD is distinguished by its large Mn reserve (>200 × 10^6 tonnes, Liu et al., 2017) and can provide a natural laboratory for understanding the formation of MSMDs. A curious feature of these deposits is that they formed coincident with the eruption of the nearby Emeishan Large Igneous Province (ELIP). Large-scale volcanism could release a large amount of Mn into the ocean and provide a fundamental metal source for the MSMDs (Chen et al., 2018). As well, volcanism could release large volumes of greenhouse gases (e.g., CO_2) into the atmosphere, leading to global warming, enhanced silicate weathering as well as enhanced input of terrestrial nutrients into the

* Corresponding authors at: State Key Laboratory of Ore Deposit Geochemistry, Institute of Geochemistry, Chinese Academy of Sciences, Guiyang 550081, China (R. Yin).
E-mail addresses: yinrunsheng@mail.gyig.ac.cn (R. Yin), gaojunbo1985@126.com (J. Gao).

https://doi.org/10.1016/j.oregeorev.2023.105530
Received 25 December 2022; Received in revised form 29 April 2023; Accepted 2 June 2023
Available online 8 June 2023

ocean. This could promote oceanic productivity, resulting in elevated dissolved O_2 levels in the surface ocean while developing anoxic conditions in the deep ocean (Yan et al., 2020). A frequent exchange between O_2-rich surface water and O_2-poor deep water might favor the oxidization of Mn^{2+} in deep waters to form MSMDs (Post, 1999; Armstrong, 2008). As such we hypothesize that the ELIP eruption may have been an important driving force for the genesis of Middle Permian MSMDs in South China, and test this hypothesis by examining MSMD depots for fingerprints of volcanism.

Mercury (Hg) is a useful proxy of large-scale volcanism in geological history (Grasby et al., 2019) as volcanism is the primary source of Hg in the environment (Selin, 2009; Grasby et al., 2017). Large-scale volcanism can transiently emit large amounts of Hg, which when transported globally in the atmosphere can be deposited in oceans and on land, leading to anomalously high Hg levels in global sediments (Grasby et al., 2020). Mercury stable isotopes (^{196}Hg, $^{198\text{-}202}$Hg, and ^{204}Hg), undergo both mass-dependent fractionation (MDF, normally reported as δ^{202}Hg) and mass-independent fractionation (MIF, normally reported as Δ^{199}Hg. Unlike that Hg-MDF occurs during a variety of physical, chemical, and biological processes, Hg-MIF mainly occurs during photochemical reactions with limited influence from other processes (Bergquist and Blum, 2007; Blum et al., 2014). Aqueous Hg(II) photoreduction process on Earth's surface leads to negative Δ^{199}Hg values of gaseous Hg(0) and positive Δ^{199}Hg values of aqueous Hg(II) species (Bergquist and Blum, 2007). Sedimentation, diagenesis, and metamorphism processes do not trigger Hg-MIF, allowing the use of Δ^{199}Hg in sedimentary records for understanding Hg geochemical cycles in geological history (Grasby, et al., 2019; Chen et al., 2022; Liu et al., 2022). Volcanic Hg derived from the primitive mantle has Δ^{199}Hg of ~ 0‰ (Moynier et al., 2021; Yin et al., 2022). This signature can be altered by photochemical reactions on Earth's surface, resulting in negative Δ^{199}Hg values (-0.6 to 0‰) in terrestrial reservoirs (e.g., soil and vegetation) and positive Δ^{199}Hg values (0 to 0.4‰) in marine reservoirs (e.g., seawater and sediments) (Blum et al., 2014). While directly increasing the atmospheric flux of Hg to oceans, large-scale volcanism can also cause profound environmental perturbations, leading to enhanced silicate weathering and soil erosion that in turn increases the input of terrestrial Hg to the ocean. Such enhanced terrestrial input is reflected by negative excursions of Δ^{199}Hg associated with Hg spikes in coastal sediments deposited during large-scale volcanic eruptions (Grasby et al., 2017; Them et al., 2019; Zhou et al., 2021). Environmental perturbations caused by LIP events are also associated with changes in sediment trace

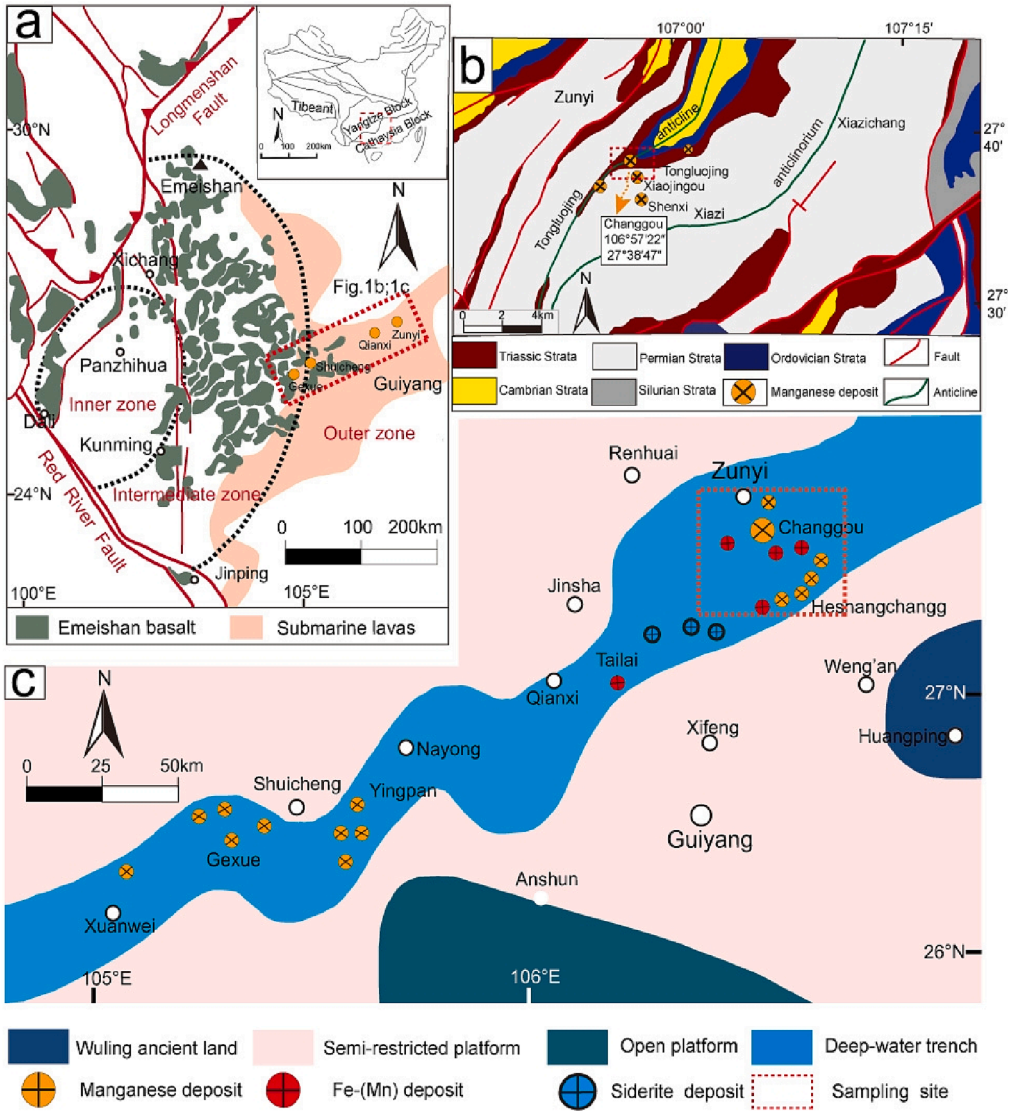

Fig. 1. (a) Simplified distribution map showing the Emeishan Large Igneous Province (ELIP) in southwestern China (after Shellnutt, 2014); (b) Regional geological map showing the Middle Permian Zunyi sedimentary manganese deposit (after Liu et al., 2015). (c) Lithofacies and paleogeography in central-western Guizhou during the Middle to Late Permian (after Chen et al., 2003b).

element concentrations. Anomalously high Li, Zr, Nb, and Ta levels in sediments are reflective of enhanced terrestrial erosion (Kısakűrek et al., 2005; Dai et al., 2018), whereas anomalous Zn, Cd, Mo, and U concentrations in sediments are indicative of changes in oceanic productivity and redox condition (Chang et al., 2009).

Here, we measured Hg concentrations and isotopic compositions of samples collected from the Zunyi MSMD. Combining our new results with available trace element data, from the same samples, we demonstrate that the ELIP eruption caused profound changes in the land–ocean-climate system that drove the formation of MSMDs in South China.

2. Geological background

2.1. Regional geology

The regional geology of South China during the Middle Permian is shown in Fig. 1**a** and has been described in detail by Gao et al. (2018). In brief, the Dongwu Uplift Movement (DUM) was a major tectonic event in the Permian of South China. The DUM was characterized by extensional rifting, continuous crustal thinning, and fracturing. Central faults in the rift zone cut through the crust to the top of the asthenosphere, resulting in the eruption of the ELIP at ~ 260.55 ± 0.07 Ma to 257.22 ± 0.37 Ma (Huang et al., 2022) and the formation of a rifting basin in South China (Xu et al., 2013; Yan et al., 2020). In the basin, shallow-water carbonate platform deposition (carbonate successions) mainly occurred in Northern Guizhou and Eastern Yunnan, and deep-water platform gullies (sedimentary siliceous rocks and limestones) mainly occurred in a NE–SW trending zone in central Guizhou (Chen et al., 2003a). A large number of Permian MSMDs, including the Zunyi MSMD (Fig. 1**b and c**), were found in the deep-water platform gullies in central Guizhou. These MSMDs contain mainly manganese carbonate minerals (e.g., rhodochrosites, calcimangite, capillitite, manganocalcite, and kutnohorite) (Liu et al., 2015; Gao et al., 2018).

2.2. Ore deposit geology

Cambrian, Ordovician, Silurian, Permian, and Triassic strata outcrop in the Zunyi area (Fig. 1**b**). The Upper Cambrian Loushanguan Formation mainly consists of dolomite. Silurian rocks are mainly siltstone and shale. Ordovician rocks are mainly dolomite and bioclastic limestone. The Permian strata consist mainly of siliceous rock, carbonaceous mudstone, and limestone. The Triassic strata consist mainly of mudstone, marlite, and dolomite. The Zunyi MSMD is located in the Permian Maokou Formation, which consists of three lithological members (Fig. 3): Member I consists mainly of carbonaceous-siliceous limestone; Member II consists mainly of Mn-bearing rocks; Member III consists mainly of limestone. Mn-bearing rocks hosted in Member II show lamellar, massive, banded, fragmental, and pisolitic structures (Xu et al., 2021).

The Zunyi MSMD contains various manganese ore types. Lamellar, clastic, massive, and pisolitic structures are commonly found in the ores (Fig. 2**a**–**d**). The mineral composition of the Mn ores is relatively simple, with the main Mn-bearing minerals being rhodochrosite and, to a lesser degree, Mn-rich calcite (Gao et al., 2018). The mineralogical features of the Mn ores have been studied using a scanning electron microscope. Irregular granular or laminar pyrites of micrometer size are occasionally found in association with rhodochrosite (Fig. 2**e**–**f**).

3. Analytical methods

Samples were collected from the Maokou Formation in the Changgou section of the Zunyi MSMD (Fig. 1**c**). The collected samples include three carbonaceous-siliceous limestones, three carbonaceous mudstones, four carbonaceous mudstones, and tuffaceous claystone, six Mn ore-bearing carbonates and one limestone. The lithologic information and spatial relationship of the samples are shown in Table S1 and Fig. 3. The samples were rinsed with deionized water, air-dried, polished to powders, sieved to 150 mesh, and homogenized, prior to chemical analyses.

3.1. Total organic carbon analysis

Total organic carbon (TOC) concentration was measured at ALS Minerals, Guangzhou, China. Briefly, the inorganic carbon in the weighed sample powders (~200 mg) was first removed by adding 10% HCl at 60 °C. The samples were then rinsed with distilled water, dried at 50 °C overnight, and used for TOC analyses with a LECO CS 230 carbon and sulfur analyzer. This method yielded an analytical uncertainty of < 5% for TOC concentration.

3.2. Hg concentration and isotopic composition analysis

Mercury concentrations of the samples were measured using a Lumex RA-915 + Hg analyzer equipped with a PYRO-915 + attachment (Russia) at the Institute of Geochemistry, Chinese Academy of Sciences (IGCAS), with a detection limit of 0.5 ng/g. Standard reference material GSS-4 (yellow soil) was simultaneously tested and yielded THg recoveries of 90 to 110%. Analyses of sample duplicates yielded an uncertainty of < 10%. Based on the measured THg concentrations, sample powders containing 25 ng Hg were weighed for Hg pre-concentration into 5 mL of 40% reverse aqua regia (HCl/HNO_3 = 1/3, v/v), using a double-stage tube furnace (Zerkle et al., 2020). GSS-4 was prepared in the same way as the samples. The preconcentrated solutions were diluted to 0.5 ng/mL Hg and measured by a Neptune Plus multi-collector inductively coupled plasma–mass spectrometer at the IGCAS, following the methods of Yin et al. (2016). Hg isotope compositions were reported following the standard convention (Blum and Bergquist, 2007). MDF is expressed in $\delta^{202}Hg$ notation in units of ‰ referenced to NIST-3133 Hg standard (analyzed before and after each sample):

$$\delta^{202}Hg(‰) = [(^{202}Hg/^{199}Hg_{sample})/(^{202}Hg/^{199}Hg_{NIST\text{-}3133}) - 1] \times 1000.$$

MIF is reported in Δ notation, which represents the differences between the measured $\delta^{xxx}Hg$ and the theoretically predicted $\delta^{xxx}Hg$, in units of ‰:

$$\Delta^{xxx}Hg = \delta^{xxx}Hg - \delta^{xxx}Hg \times \beta.$$

β is 0.252 for ^{199}Hg, 0.5024 for ^{200}Hg, and 0.7520 for ^{201}Hg. NIST 3177 secondary standard solution, diluted to 0.5 ng/mL Hg in 10% HCl (v/v), was measured in every 10 samples to monitor the data quality. The overall average and uncertainty of NIST-3177 ($\delta^{202}Hg$ = -0.54 ± 0.13‰; $\Delta^{199}Hg$ = -0.01 ± 0.09‰; $\Delta^{200}Hg$ = 0.01 ± 0.03‰; $\Delta^{201}Hg$ = 0.01 ± 0.06‰; 2SD, n = 3) and GSS-4 ($\delta^{202}Hg$ = -1.77 ± 0.08‰; $\Delta^{199}Hg$ = -0.43 ± 0.08‰; $\Delta^{200}Hg$ = -0.03 ± 0.06‰; $\Delta^{201}Hg$ = 0.37 ± 0.07‰; 2SD, n = 3) are in good agreement with the reported values (Blum and Bergquist, 2007; Chen et al., 2022).

3.3. Principal component analysis

Principal component analysis (PCA) is a multivariate, statistical, and exploratory analysis method that can be used in the interpretation of a many-variable data matrix (Webster, 2001). In this method, the chemical species are combined according to their provenance in the formation environment in a matrix of geochemical data. Therefore, new data from these linear combinations are derived, forming the principal components which can be displayed as scores and weights. Factor scores indicate how strongly individual samples are associated with each of the factors, and thus can be used to investigate similarity between samples, where samples with a similar composition will have similar scores and may therefore have similar sources and behavior. We constructed PCAs of our results using the OriginLab 2021 software. The operation is as follows: Import trace element contents of studied samples into OriginLab 2021 software, select the imported trace element content data table,

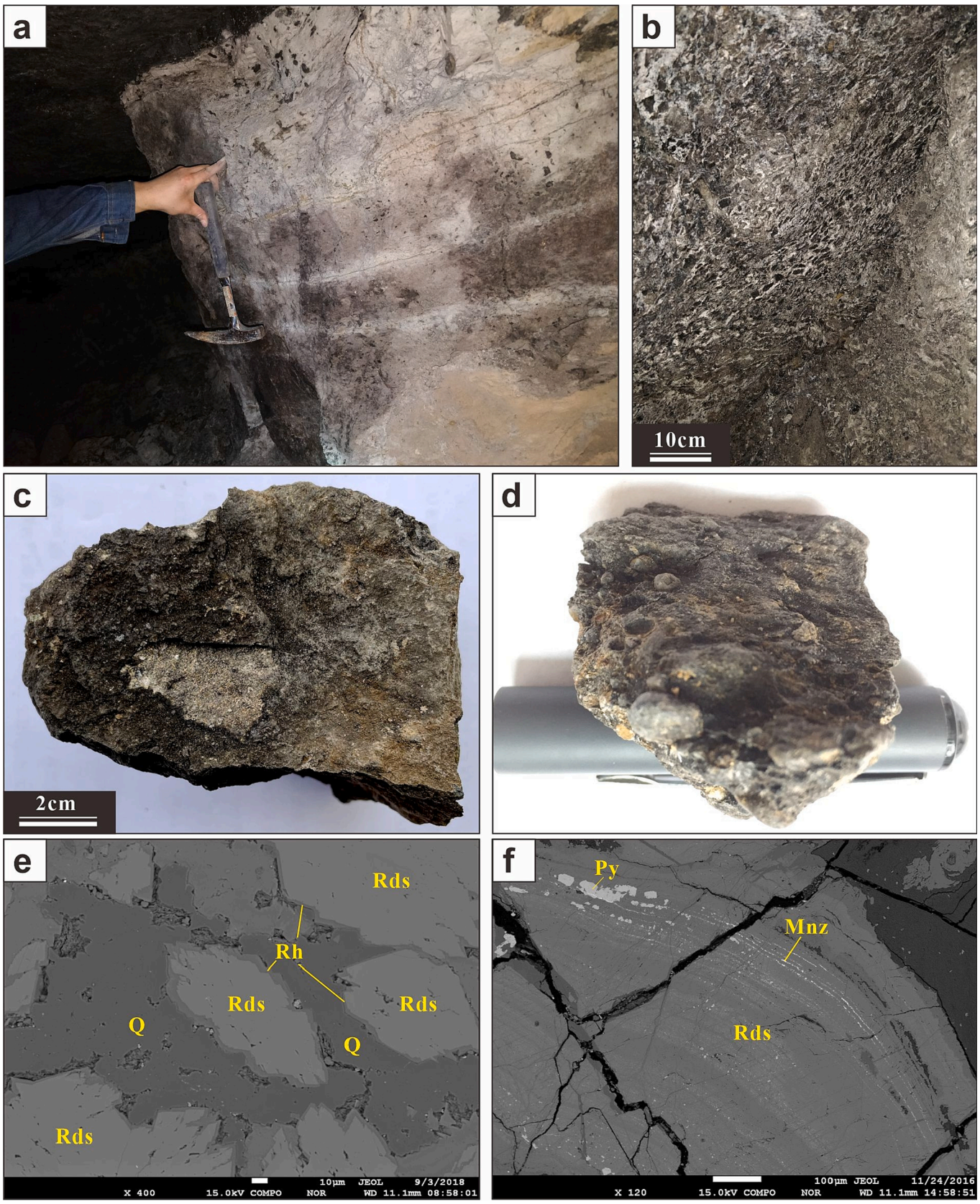

Fig. 2. Photographs showing typical features and microstructure of the Zunyi manganese deposit, South China. (a) Manganese ore body showing lamellar structure; (b) Manganese ore showing clastic structure; (c) Manganese ore showing dense massive structure; (d) pisolitic manganese ore; (e) Irregular globular rhodochrosite surrounded by capillitite (SEM view); (f) Lamellar rhodochrosite, with micrometer scales monazite distributed along the bedding(SEM view). Py: pyrite; Rds: rhodochrosite; Q: quartz; Mnz: monazite.

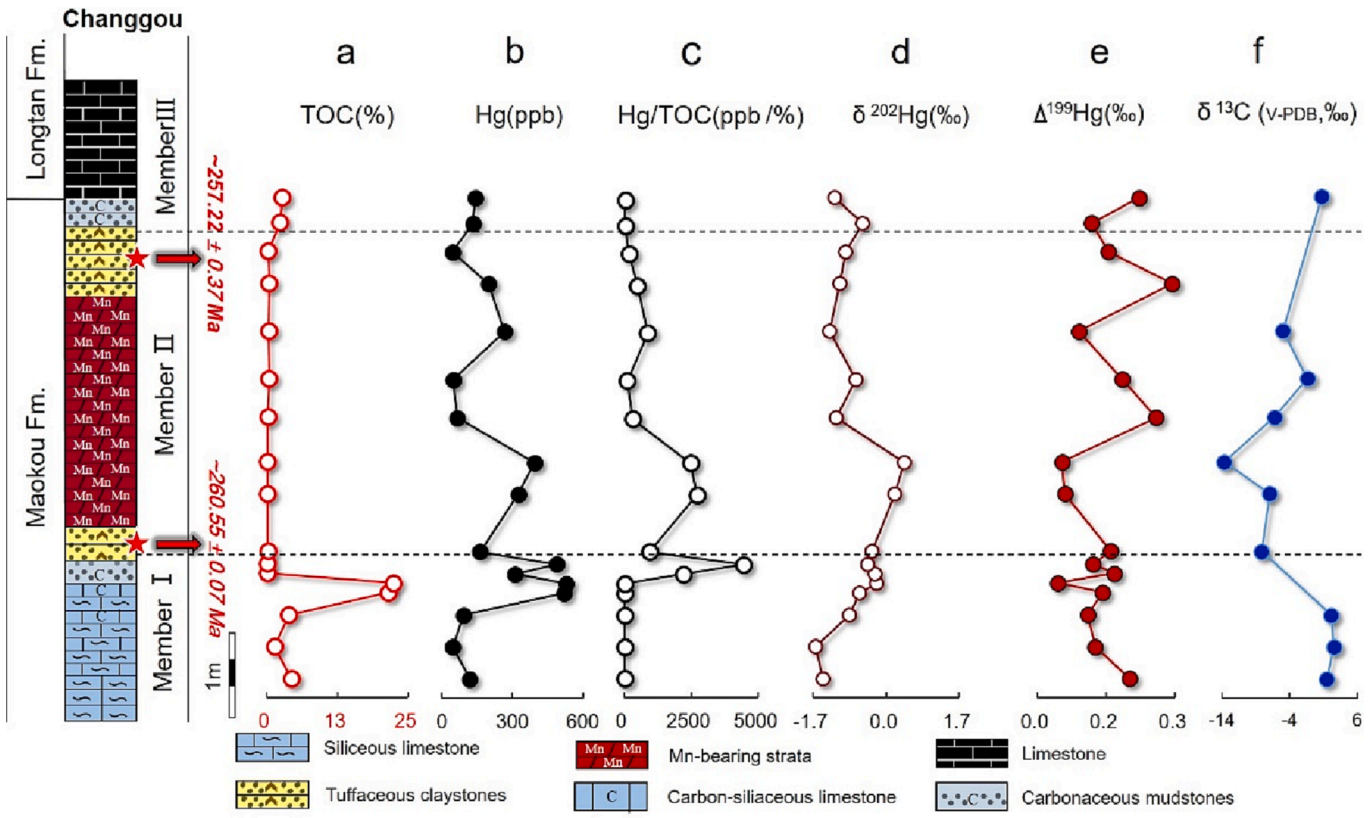

Fig. 3. Stratigraphic column for the Changgou section in the Middle Permian Zunyi sedimentary manganese deposit, Guizhou, South China (after Gao et al., 2018; age comes from Yan et al., 2020; Shellnutt et al., 2020) and vertical variation of TOC (a), Hg (b), Hg/TOC (c), δ^{202}Hg (d), Δ^{199}Hg (e) and $\delta^{13}C_{carb}$ (f, after Xu, 2021).

select statistical command in the command window or interface, select multivariate analysis, and then select principal component analysis, click the pop-up window after the command to set parameters. Loading on one variable close to ± 1 indicates a strong correlation between a variable and the factor. Variables that exhibited a loading > 0.5 were considered significant.

4. Results

4.1. Total organic carbon concentrations

TOC concentrations of the samples (Supplementary Table S1) are shown in Fig. 3. The TOC values of Members I, II, and III samples in the Maokou Formation range from 1.36 to 4.34 wt%, 0.11 to 22.4 wt%, and 2.36 to 2.7 wt%, respectively. The TOC concentrations are mostly lower than 3 wt% throughout the Maokou Formation, but a sudden peak can be observed at the boundary of Members I and II (Fig. 3).

4.2. Hg concentrations and isotopic compositions

Hg concentrations and isotopic compositions of the samples (Supplementary Table S1) are shown in Fig. 3. Hg concentrations range from 47.1 to 118 ppb, 44.9 to 531 ppb, and 133 to 141 ppb for samples in Members I, II, and III, respectively. Hg/TOC ratios range from 23.5 to 34.6 ppb/wt.%, 23.7 to 4430 ppb/wt.%, and 52.3 to 56.3 ppb/wt.% for samples in Members I, II, and III, respectively. Anomalously high Hg concentrations and Hg/TOC ratios can be found at the boundary of Members I and II. Samples in Member I show negative δ^{202}Hg values of −1.64 to −0.85‰ and positive Δ^{199}Hg values of 0.11 to 0.20‰. Member II samples show an increase of δ^{202}Hg from −1.31 to 0.43‰ and a decrease in Δ^{199}Hg values from 0.29 to 0.04‰. Member III shows negative δ^{202}Hg of −1.20 to −0.54‰ and positive Δ^{199}Hg of 0.12 to 0.22‰.

4.3. Trace elements

Trace elements of the same samples have been reported in a recent study (Xu et al., 2021). Further processing of these data, as part of this study, through Principal Component Analysis (PCA) revealed three clusters of trace elements associated with different distribution patterns (Fig. 4).

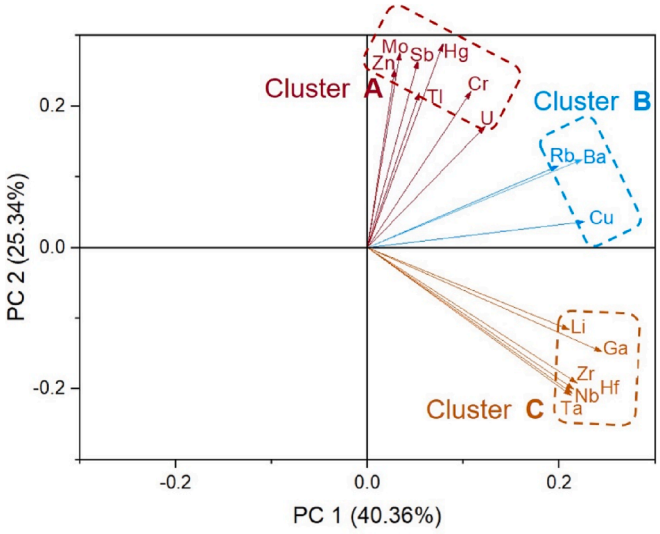

Fig. 4. PC1 versus PC2 scatter plot (the element distance between elements indicates the strength of the correlation).

Cluster A elements (Cr, Ni, Zn, Mo, Sb, Tl, and U) in all samples are positively correlated with each other (R = 0.35 to 0.83, p < 0.05). Peak concentrations of Cluster A elements are found at the boundary of Members I and II (Fig. 5), similar to that observed for Hg concentrations and Hg/TOC ratios.

Cluster B elements (Cu, Rb, and Ba) in all samples are also positively correlated with each other (R = 0.56 to 0.92, p < 0.05), and they show relatively lower concentrations in Member I samples than in Members II and III samples. In particular, a sudden peak of Cluster B elements can be found at the boundary of Members I and II (Fig. 6).

Cluster C elements (Li, Ga, Zr, Nb, Hf and Ta) in all samples positively correlate with each other as well (R = 0.66 to 1, p < 0.05), and they show a stepwise increase from Members I, II to III (Fig. 7).

5. Discussion

5.1. Large-scale volcanism occurred prior to the deposition of the Zunyi MSMD

Anomalously high Hg concentrations and Hg/TOC ratios can be indicative of large-scale volcanism in geological history (Grasby et al., 2019). In this study, the peaks of Hg concentrations and Hg/TOC ratios at the boundary of Members I and II suggest the presence of large-scale volcanism prior to the formation of the Zunyi MSMD that is within Member II. Tuff and basalts containing zircons of ~ 260 Ma have been found at the boundary of Members I and II at our study site (Fig. 3) and some other sites in South China, which are attributed to the ELIP eruption (Yan et al., 2020). Mercury isotopes support the origin of these Hg anomalies being related to large-scale volcanism. Volcanic Hg derived from the primitive mantle has Δ^{199}Hg of ~ 0‰ (Moynier et al., 2021; Yin et al., 2022). The shift to near-zero Δ^{199}Hg at the boundary of Members I and II (Fig. 3) may be explained by the deposition of Hg emitted from the ELIP, due to the proximity between ELIP and the Zunyi MSMD (Fig. 1).

Besides Hg, Cluster A elements (Cr, Zn, Mo, Sb, and Tl) are enriched in volcanic plumes (Mandon et al., 2019). The positive correlation between Hg and most Cluster A elements (R = 0.23 to 0.95, p < 0.05) supports a similar origin (Fig. 8). Anomalous concentrations of Cluster A elements occur at the boundary of Member I and II (Fig. 5), at the same level as the Hg anomalies. This further supports that large-scale volcanism occurred at this time.

5.2. Strong continental weathering during the formation of the Zunyi MSMD

Cluster C elements are typical indicators of continental weathering (Horbe and Da Costa, 1999; Kısakűrek et al., 2005; Dai et al., 2018). The stepwise increase of Cluster C elements (Li, Ga, Zr, Nb, Hf, Ta) in Members II and III samples (Fig. 6) supports enhanced continental weathering during the formation of the Zunyi MSMD. Consistent with our study, previous studies also demonstrated elevated chemical index of alteration (CIA) in Member II samples (Xu et al., 2021). Key here is that this signal occurs after the Hg and other geochemical anomalies suggestive of large-scale volcanism.

Enhanced continental weathering is mostly associated with global warming and elevated atmospheric CO_2 levels. Large-scale volcanism could emit large amounts of CO_2 that contribute to global warming (Lee et al., 2015). The volume of the ELIP basalts has been estimated to be at least 0.3 × 10^6 km^3 (Shellnutt, 2014). A simple calculation of 100% degassing of 0.5 wt% CO_2 injects approximately 3.5 Mt(C) per/km^3 of magma (Self et al., 2005). Using the same assumption of the CO_2 content of magma gives the potential release of 1050 Gt carbon from the ELIP, which could cause perturbations to the carbon cycle and trigger global warming. Negative $\delta^{13}C_{carb}$ excursions have been previously observed in Maokou Member II samples (Xu, 2021), suggesting that ELIP eruption could have had a profound impact on the C cycle during this time, likely due to the release of massive amounts of ^{13}C-depleted CO_2 by magmatic degassing (Yang et al., 2018; Sun et al., 2022).

5.3. Enhanced oceanic productivity and surface ocean oxygenation during the formation of Zunyi MSMD

Cluster B elements (Ba, Rb, and Cu), indicative of high oceanic productivity, are often enriched in MSMDs (Boström, 1983; Marchig

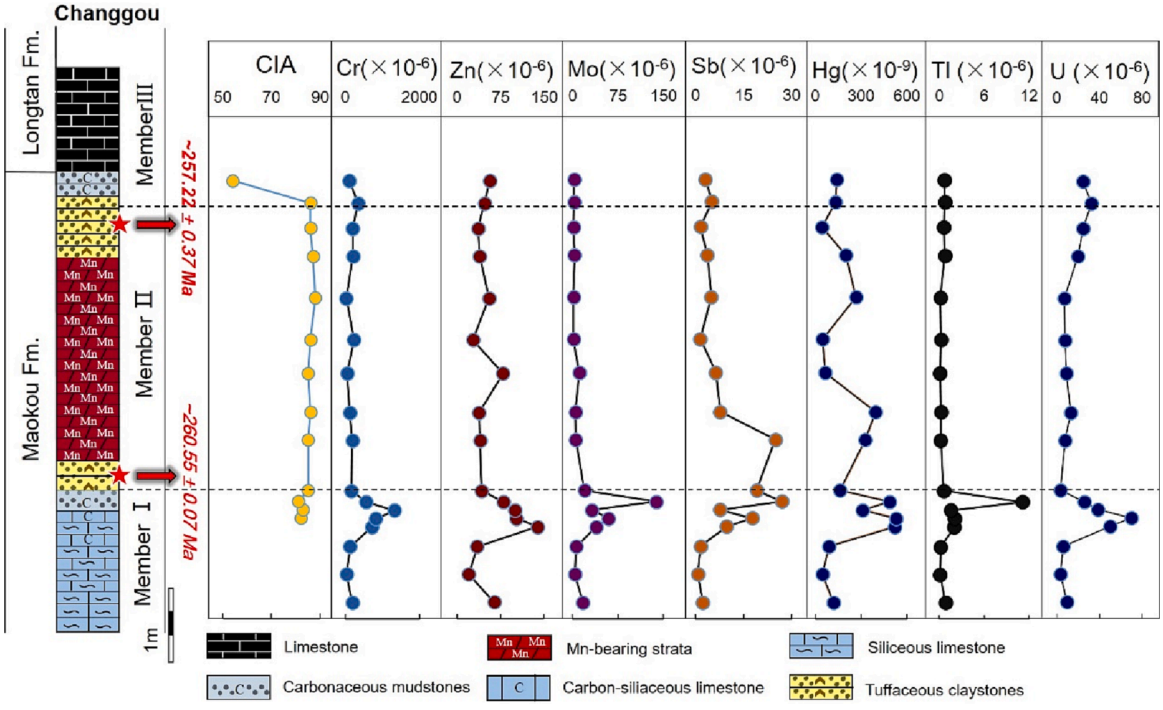

Fig. 5. Vertical changes in Cluster A elements (Cr, Zn, Mo, Sb, Hg, TI, and U) in the Changgou section, Guizhou, China.

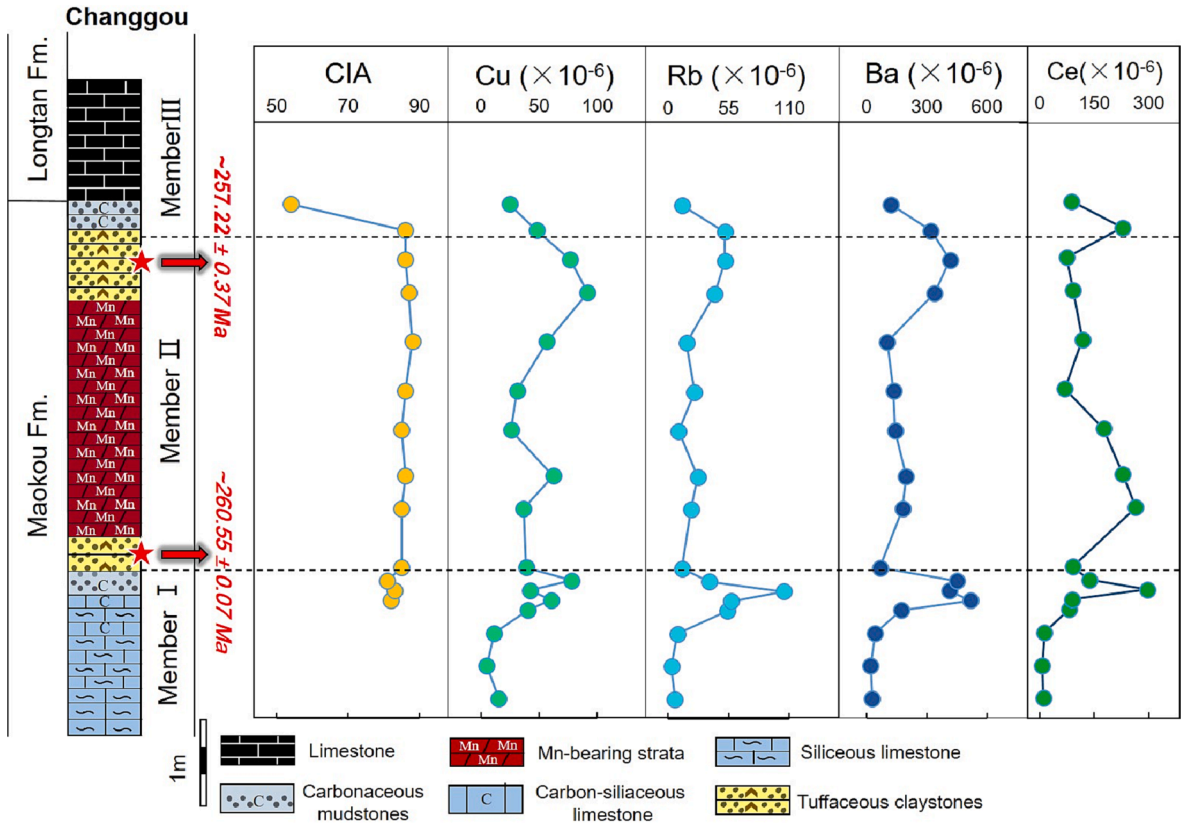

Fig. 6. Vertical changes in Cluster B elements (Cu, Rb, Ba), Ce content (after Xu, 2021), and CIA values (after Xu, 2021) in the Changgou section, Guizhou, China.

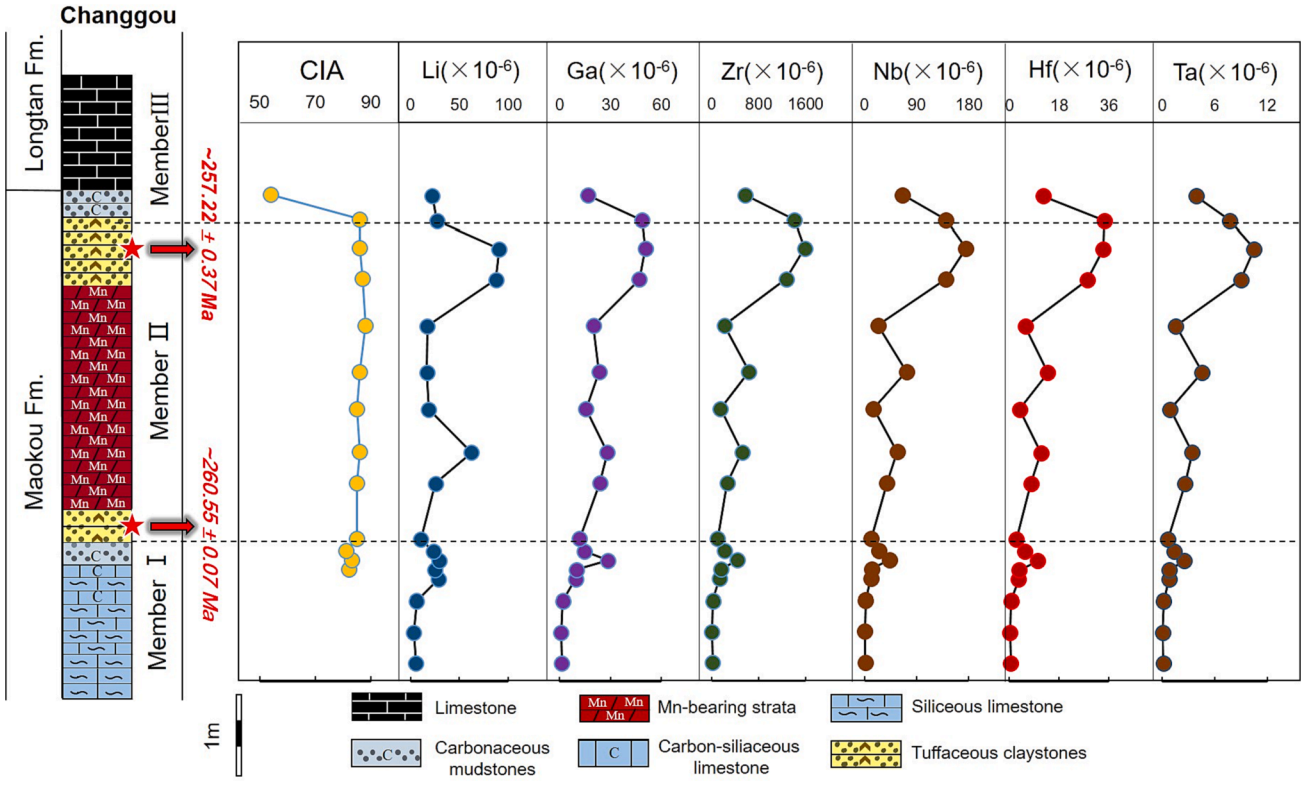

Fig. 7. Vertical changes in Cluster C elements (Li, Ga, Zr, Nb, Hf, and Ta) and CIA values (after Xu, 2021) in the Changgou section, Guizhou, China.

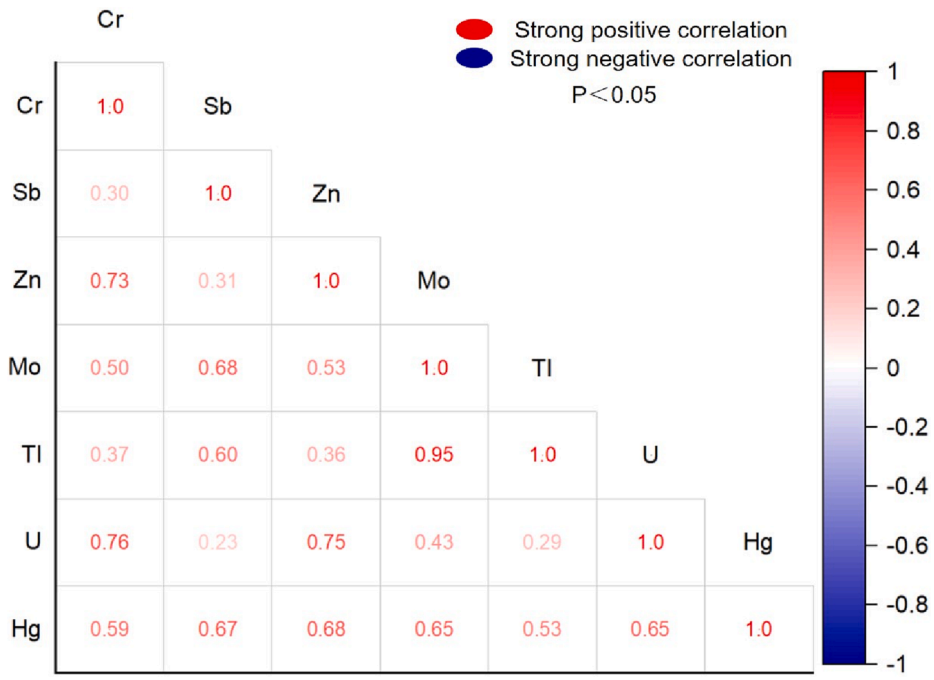

Fig. 8. Coefficients of correction between Hg and Group A elements.

et al., 1982; Xie et al., 2013). The increase of Cluster B elements in Member II samples (Fig. 7) suggests that marine productivity was enhanced during the deposition of the Zunyi MSMD. The increase in marine productivity should lead to an increase in the dissolved O_2 in the surface seawater, which would facilitate the deposition of Mn, as discussed below. According to Xu et al. (2021), the Ce_{anom} values of the studied samples support that the redox condition evolved from anoxic in Member I to suboxic or oxic in Members II and III.

6. Conclusions and implications for the genesis of the Zunyi MSMD

Results of this study provide insights into the genesis of the Zunyi MSMD and the climate-ocean-land dynamics in South China during the Middle Permian. ELIP eruption, as revealed by anomalously high Cluster A elements concentrations and Hg/TOC ratios at the boundary of Members I and II, released large volumes of CO_2 into the atmosphere, triggering enhanced terrestrial weathering, as supported by the stepwise increase in Cluster C elements concentrations in Member II. Enhanced terrestrial weathering facilitated input of terrestrial nutrients to the ocean as well, which would increase oceanic productivity, as supported by elevated concentrations of Cluster B elements in Member II. Elevated oceanic productivity in Member II would increase dissolved O_2 levels in the surface ocean via photosynthesis ($CO_2 + H_2O \rightarrow CH_2O + O_2$), resulting in enhanced organic matter shuttle to the seafloor as well. Dissolved O_2 in seawater favor MnO_2 deposition to sediments. During sedimentary diagenesis, MnO_2 would readily react with organic matter to form abundant carbonate Mn-bearing minerals (e.g., rhodochrosites, calcimangite, capillitite, manganocalcite, and kutnohorite) (Wu et al., 2016). Overall, this study highlights that the ELIP eruption could have played an important role in causing profound changes in the land–ocean-climate system, and would be a driving force for the formation of Middle Permian MSMDs in South China.

Declaration of Competing Interest

The authors declare that they have no known competing financial interests or personal relationships that could have appeared to influence the work reported in this paper.

Data availability

Data will be made available on request.

Acknowledgment

This work was supported by the National key research and development program (2022YFC2903403).

Appendix A. Supplementary data

Supplementary data to this article can be found online at https://doi.org/10.1016/j.oregeorev.2023.105530.

References

Armstrong, F.A., 2008. Why did nature choose manganese to make oxygen? Philos. Trans. Royal Soc. B, Biol. Sci. 363, 1263–1270.
Bergquist, B.A., Blum, J.D., 2007. Mass-dependent and-independent fractionation of Hg isotopes by photoreduction in aquatic systems. Science 318, 417–420.
Blum, J.D., Bergquist, B.A., 2007. Reporting of variations in the natural isotopic composition of mercury. Anal. Bioanal. Chem. 388, 353–359.
Blum, J.D., Sherman, L.S., Johnson, M.W., 2014. Mercury isotopes in earth and environmental sciences. Annu. Rev. Earth Planet. Sci. 42, 249–269.
Boström, K., 1983. Genesis of ferromanganese deposits–diagnositc criteria for recent and old deposits. In: Rona, P.A., Boström, K., Laubier, L. (Eds.), Hydrothermal Processes at Seafloor Spreading Centers. Plenum Press, New York, pp. 473–489.
Chang, H.J., Chu, X.L., Feng, L.J., et al., 2009. Redox sensitive trace elements as paleoenvironments proxies. Geol. Rev. 55 (1), 91–99.
Chen, W., Liu, J., Wang, Z., et al., 2003. Study on lithofacies palaeogeography during the Permian Emeishan basalt explosion in Guizhou Province. J. Palaeogeogr. 5 (1), 17–28.
Chen, W.Y., Liu, J.R., Wang, Z.G., Zheng, Q.L., 2003. During the Permian Emeishan basalt explosion in Guizhou Province. J. Palaeogeogr. 5, 17–28 (in Chinese with English abstract).
Chen, D., Ren, D., Deng, C., et al., 2022. Mercury loss and isotope fractionation during high-pressure and high-temperature processing of sediments: Implication for the behaviors of mercury during metamorphism. Geochim. Cosmochim. Acta 334, 231–240.
Chen, F.G., Wang, Q.F., Yang, S.J., Zhang, Q.Z., Liu, X.F., Chen, J.H., Carranza, E.J.M., 2018. Space time distribution of manganese ore deposits along the southern margin of the South China Block, in the context of Palaeo-Tethyan evolution. Int. Geol. Rev. 60, 72–86.

Dai, S., Nechaev, V.P., Chekryzhov, I.Y., et al., 2018. A model for Nb–Zr–REE–Ga enrichment in Lopingian altered alkaline volcanic ashes: Key evidence of HO isotopes. Lithos 302, 359–369.
Entr, D., 2014. Report on critical raw materials for the EU. European Commission, Brussels, Belgium.
Gao, J., Yang, R., Xu, H., et al., 2018. Genesis of Permian sedimentary manganese deposits in Zunyi, Guizhou Province, SW China: Constraints from geology and elemental geochemistry. J. Geochem. Explor. 192, 142–154.
Grasby, S.E., Shen, W., Yin, R., Gleason, J.D., Blum, J.D., Lepak, R.F., Hurley, J.P., Beauchamp, B., 2017. Isotopic signatures of mercury contamination in latest Permian oceans. Geology 45, 55–58.
Grasby, S.E., Them, T.R., Chen, Z., Yin, R., Ardakani, O.H., 2019. Mercury as a proxy for volcanic emissions in the geologic record. Earth-Sci. Rev. 196.
Grasby, S.E., Liu, X., Yin, R., Ernst, R.E., Chen, Z., 2020. Toxic mercury pulses into late Permian terrestrial and marine environments. Geology 48, 830–833.
Hem, J.D., 1972. Chemical factors that influence the availability of iron and manganese in aqueous systems. Geol. Soc. Am. Bull. 83 (2), 443–450.
Horbe, A.M.C., Da Costa, M.L., 1999. Geochemical evolution of a lateritic Sn–Zr–Th–Nb–Y–REE-bearing ore body derived from apogranite: the case of Pitinga, Amazonas—Brazil. J. Geochem. Explor. 66 (1–2), 339–351.
Huang, H., Huyskens, M.H., Yin, Q.Z., et al., 2022. Eruptive tempo of Emeishan large igneous province, southwestern China and northern Vietnam: Relations to biotic crises and paleoclimate changes around the Guadalupian-Lopingian boundary. Geology 50 (9), 1083–1087.
Kısakűrek, B., James, R.H., Harris, N.B.W., 2005. Li and δ7Li in Himalayan rivers: proxies for silicate weathering? Earth Planet. Sci. Lett. 237 (3–4), 387–401.
Lee, C.-T.A., Thurner, S., Paterson, S., Cao, W., 2015. The rise and fall of continental arcs: interplays between magmatism, uplift, weathering, and climate. Earth Planet. Sci. Lett. 425, 105–119.
Liu, Z., Tian, H., Yin, R., Chen, D., Gai, H., 2022. Mercury loss and isotope fractionation during thermal maturation of organic-rich mudrocks. Chem. Geol. 612.
Liu, Z.C., Yan, J.X., et al., 2017. Main progress and potential prediction of geological prospecting of manganese ore in national fully equipped exploration area of Zunyi, Guizhou Province. Guizhou Geol. 34 (2), 8. In Chinese with English abstract.
Liu, Z.C., Wang, C., Zhang, Y.G., et al., 2015. Geochemistry and ore genesis of Zunyi Mn deposit, Guizhou Province, China. Acta Mineral. Sin 35 (4), 481–488.
Mandon, C.L., Christenson, B.W., Schipper, C.I., et al., 2019. Metal transport in volcanic plumes: a case study at White Island and Yasur volcanoes. J. Volcanol. Geoth. Res. 369, 155–171.
Marchig, V., Gundlach, H., Möller, P., Schley, F., 1982. Some geochemical indicators for discrimination between diagenetic and hydrothermal metalliferous sediments. Mar. Geol. 50, 241–256.
Moynier, F., Jackson, M.G., Zhang, K., et al., 2021. The mercury isotopic composition of Earth's mantle and the use of mass independently fractionated Hg to test for recycled crust. Geophys. Res. Lett. 48 (17) e2021GL094301.
Murray, J.W., Dillard, J.G., Giovanoli, R., Moers, H., Stumm, W., 1985. Oxidation of Mn (II): initial mineralogy, oxidation state and ageing. Geochim. Cosmochim. Acta 49, 463–470.
Post, J.E., 1999. Manganese oxide minerals: crystal structures and economic and environmental significance. Proc. Natl. Acad. Sci. U. S. A. 96, 3447–3454.
Self, S., Thordarson, T., Widdowson, M., 2005. Gas fluxes from flood basalt eruptions. Elements 1, 283–287.
Selin, N.E., 2009. Global biogeochemical cycling of mercury: a review. Annu. Rev. Env. Resour. 34, 43–63.
Shellnutt, J.G., 2014. The Emeishan large igneous province: a synthesis. Geosci. Front. 5, 369–394.
Shellnutt, J.G., Pham, T.T., Denyszyn, S.W., et al., 2020. Magmatic duration of the Emeishan large igneous province: Insight from northern Vietnam[J]. Geology 48 (5), 457–461.
Sun, S., Chen, A., Hou, M., et al., 2022. Rapid climatic fluctuations during the Guadalupian-Lopingian transition: implications from weathering indices recorded in acid-insoluble residues of carbonate rocks, South China. J. Asian Earth Sci. 230.
Tang, J.R., Yang, Z.X., Zhou, P., Shi, J.F., 2014. The progress in the strategic study of critical minerals and its implications. Geol. Bull. China 33 (9), 1445–1453. In Chinese with English abstract.
Thamdrup, B., Rosselló-Mora, R., Amann, R., 2000. Microbial manganese and sulfate reduction in Black Sea shelf sediments. Appl. Environ. Microbiol. 66, 2888–2897.
Them, T.R., Jagoe, C.H., Caruthers, A.H., et al., 2019. Terrestrial sources are mercury's primary delivery mechanism to the oceans across the Toarcian Oceanic Anoxic Event (Early Jurassic). Earth Planet. Sci. Lett. 507, 62–72.
Webster, T.J., 2001. A principal component analysis of the US News & World Report tier rankings of colleges and universities. Econ. Educ. Rev. 20 (3), 235–244.
Wu, C., Zhang, Z., Xiao, J., Fu, Y., Shao, S., Zheng, C., Xiao, C., 2016. Nanhuan manganese deposits within restricted basins of the southeastern Yangtze Platform, China: constraints from geological and geochemical evidence. Ore Geol. Rev. 75, 76–99.
Xie, J.C., Sun, W.D., Du, J.G., Xu, W., Wu, L.B., Yang, X.Y., Zhou, T.F., 2013. Geochemical studies on Permian manganese deposits in Guichi, Eastern China: implications for their origin and formative environments. J. Asian Earth Sci. 74, 155–166.
Xu, H., 2021. the source of metallogenic materials in the Permian Manganese deposits in Northern Guizhou and Eastern Yunnan, South China And study on metallogenic mechanism. Chinese with English abstract. Guizhou University. Ph.D. dissertation thesis.
Xu, H., Gao, J., Yang, R., et al., 2021. Metallogenic mechanism of large manganese deposits from Permian manganese ore belt in western South China Block: new mineralogical and geochemical evidence. Ore Geol. Rev. 132.
Xu, Y.G., He, B., Luo, Z.Y., et al., 2013. Study on mantle plume and large igneous provinces in China: an overview and perspectives. Bull. Georgian Acad. Sci. Mineral. Petrol. Geochem. 32 (1), 25–39. In Chinese with English abstract.
Yan, H., Pi, D.H., Jiang, S.Y., et al., 2020. New constraints on the onset age of the Emeishan LIP volcanism and implications for the Guadalupian mass extinction. Lithos 360.
Yang, J., Cawood, P.A., Du, Y., et al., 2018. Early Wuchiapingian cooling linked to Emeishan basaltic weathering? Earth Planet. Sci. Lett. 492, 102–111.
Yin, R., Feng, X., Hurley, J.P., Krabbenhoft, D.P., Lepak, R.F., Hu, R., Zhang, Q., Li, Z., Bi, X., 2016. Mercury Isotopes as Proxies to Identify Sources and Environmental Impacts of Mercury in Sphalerites. Sci. Rep. 6 (1), 18686.
Yin, R., Chen, D., Pan, X., et al., 2022. Mantle Hg isotopic heterogeneity and evidence of oceanic Hg recycling into the mantle. Nat. Commun. 13 (1), 1–7.
Zerkle, A.L., Yin, R., Chen, C., Li, X., Izon, G.J., Grasby, S.E., 2020. Anomalous fractionation of mercury isotopes in the Late Archean atmosphere. Nat. Commun. 11 (1), 1709.
Zhou, T., Pan, X., Sun, R., et al., 2021. Cryogenian interglacial greenhouse driven by enhanced volcanism: evidence from mercury records. Earth Planet. Sci. Lett. 564.